Article

Assessing the Seismic Demands on Non-Structural Components Attached to Reinforced Concrete Frames

Surya Prakash Challagulla [1,*], **Denise-Penelope N. Kontoni** [2,3,*], **Ashok Kumar Suluguru** [4], **Ismail Hossain** [5], **Uppari Ramakrishna** [6] and **Mohammed Jameel** [7]

1   Department of Civil Engineering, Koneru Lakshmaiah Education Foundation, Vaddeswaram, Guntur 522302, Andhra Pradesh, India
2   Department of Civil Engineering, School of Engineering, University of the Peloponnese, GR-26334 Patras, Greece
3   School of Science and Technology, Hellenic Open University, GR-26335 Patras, Greece
4   Department of Civil Engineering, Malla Reddy Engineering College, Maisammaguda 500100, Telangana, India
5   School of Natural Sciences and Mathematics, Ural Federal University, 620000 Yekaterinburg, Russia
6   Department of Civil Engineering, Vignana Bharathi Institute of Technology, Hyderabad 501301, Telangana, India
7   Department of Civil Engineering, College of Engineering, King Khalid University, Asir, Abha 61421, Saudi Arabia
*   Correspondence: chsuryaprakash@kluniversity.in (S.P.C.); kontoni@uop.gr (D.-P.N.K.)

Abstract: Nonstructural components (NSCs) are the systems that are attached to the floors of a building structure. NSCs have become critical in sustaining post-earthquake functionality while constructing seismic-resilient structures. The seismic behavior of the NSCs primarily depends upon the behavior of the structure to which the NSC is attached. Building structures are subjected to earthquake loads and behave differently when the supporting soil type varies. In light of this, this study investigates the seismic demands on NSC attached to the floors of an elastic-reinforced concrete building frame supported by different soil types. The present study considered a regular building frame and a building frame with mass irregularity on the lower story. A total of 3 sets of 11 horizontal spectral-matched ground motions consistent with each soil type are considered. Floor response spectra (FRS) can be used to measure the seismic load on non-structural components. Primarily, it was found that the ordinates of FRS depend on the floor height, the vibration periods of the building, and the soil type. The presence of mass irregularity at the lower story amplified the floor response at all floor levels. Additionally, the values of floor spectral acceleration increase as soil flexibility increases. The amplification factors are critical for generating the floor response spectra, and their variation along the building height is discussed. The floor acceleration was found to vary non-linearly with the height of the building. Finally, artificial neural networks (ANNs) are employed to develop the prediction models for dynamic amplification factors. The results calculated by the dynamic time history analyses are utilized to validate the proposed prediction models.

Keywords: floor amplification factor; non-structural component; floor response spectra; soil type; seismic demand

1. Introduction

Non-structural components (NSCs) are elements of buildings but they do not resist loads [1]. Damage to NSCs might result in more considerable direct and indirect economic losses than principal structural members. The destruction of NSCs, including essential and expensive equipment, may affect the functioning of structures, particularly critical facilities such as hospitals, airports, and historic/culturally valuable systems [2,3]. These findings demonstrate that the seismic performances of NSCs are as important as those of structural components. The present Standards and Guidelines have been created mainly based on empirical techniques developed from prior experiences and engineering expertise [4]. Thus,

non-structural components must be earthquake-designed to keep them safe and ensure that the building can continue to function after an earthquake. In order to accomplish this, the floor response spectrum (FRS) needs to be determined at the point where the non-structural component is attached to the primary structure.

The floor response spectrum (FRS) approach is a decoupled analysis method [5–8]. The primary structure is dynamically analyzed first, without regard for the influence of the secondary system. At the floor level where the NSC is attached, the acceleration response history is used as input to a secondary structure to construct the FRS. Therefore, the maximum design force for the design of the NSCs can be obtained from the generated FRS. The seismic performance of components exposed to the ground motion was studied and it was concluded that the amplification in the response of the primary structure would increase the damage probability of NSCs [9]. In the 1970s, researchers started looking into FRS generation techniques. The NSC and its supporting structure were formerly typically treated as single degree of freedom (SDOF) systems in several methods. A novel technique is developed and validated for directly determining floor acceleration spectra [10]. Wei Jiang et al. [11] constructed floor response spectra to examine seismic demands on nuclear plants and concluded that the FRS from time history analysis had considerable variations, particularly in tuning cases. The floor response spectrum of multi-storied structures [12–17] has been investigated. Although numerous FRS generation techniques have been documented in the pertinent literature [15,18,19], none can adequately examine the effect of different soil types on the FRS.

In earthquake engineering, studying the soil type is crucial. [20]. The interaction between soil and structure has been the subject of a lot of research in recent decades because of the potential impact that soil has on structural response. [21–24]. According to Jayalekshmi and Chinmayi [25], the earthquake damages do not follow the same pattern even though the buildings are in the exact location [26]. The structure's properties solely determine the seismic response of structures built on rock. The seismic response of a building is significantly affected by the interaction between the soil and the structure when it is built on soft soil. It can produce frequency shifts and amplitude alterations in the structure's floor response spectrum [27]. As a result, the effect of different soil types should be included while developing the structural model to simulate the seismic response realistically.

In this research, an effort has been made to study the effect of various types of soil on the floor acceleration response of the regular and irregular building models. Two five-story reinforced concrete (RC) buildings are considered in this research. The NSC is modeled as an elastic SDOF system and attached to the RC building at a single point. The mass ratio (non-structural components mass to the primary structural mass) is assumed to be 0.001 for this investigation [8,28]. The decoupling analysis of primary and non-structural components (i.e., neglecting the dynamic interaction that takes place between the supporting building and the NSC) is appropriate for lighter NSCs [29]. The primary goal of this research is to assess the elastic floor acceleration response of the regular building and buildings with mass irregularity on the lower story. Such mass irregularity exists when a specific floor is used for car parking, equipment storage, etc. The floor amplification factors, peak component acceleration, component dynamic amplification factors, and floor response spectra play an essential role in assessing seismic demands on NSCs. Therefore, all the specified factors and spectra are evaluated for building models under different soil types. The amplification factors are compared with those obtained from the code-based formulations. In the generation of FRS, component dynamic amplification factors play an important role as they reflect the amplification of NSCs. Therefore, in the current study, artificial neural networks (ANNs) are employed to develop the model to predict the component dynamic amplification factors. The created ANN model is used to generate a detailed design expression. The developed ANN-based expression is compared with the literature formulation. The effectiveness of the prediction model has also been assessed

by comparing the component amplification factors computed from the ANN equation to those acquired through dynamic time history analysis of building models.

The organization of the paper can be broken down into the following sections: Section 2 describes the modeling and analysis of considered building models. The overview of the FRS is discussed in Section 3. Section 4 gives the details of the ground motion for different soil types. Section 5 presents the results and discussion. Section 6 describes the ANN model and shows the procedure to develop the prediction expression, and concise conclusions are drawn in the last section (i.e., Section 7).

2. Modeling and Analysis of Buildings

In this particular study, two five-story reinforced concrete buildings are considered, as displayed in Figure 1. The considered buildings are 2D special moment-resisting bare frames consisting of one regular building (M_R) and another building with mass irregularity (M_{IR}). In model M_{IR}, the seismic weight of the lower story (first floor) is assumed to be 200% more than that of the subsequent floor levels. As a result, the irregular building frame satisfies the IS 1893 (Part 1) [30] irregularity requirement. The structures are assumed to be in the highest seismic zone (Zone V, according to IS 1893-2016). Both frames maintain a constant 4 m bay width and 3 m story height across all stories. Steel and concrete grades used in reinforced concrete models are considered to be high-yield strength deformed bar of HYSD 415 and M30, respectively. Floor finishes and live load were set at 1 kN/m^2 and 5 kN/m^2, respectively, as per the recommendation of IS 875-Part 2 [31]. The limit state design method is used to create a frame for a medium-rise building that can withstand tributary loads up to 4 m in height.
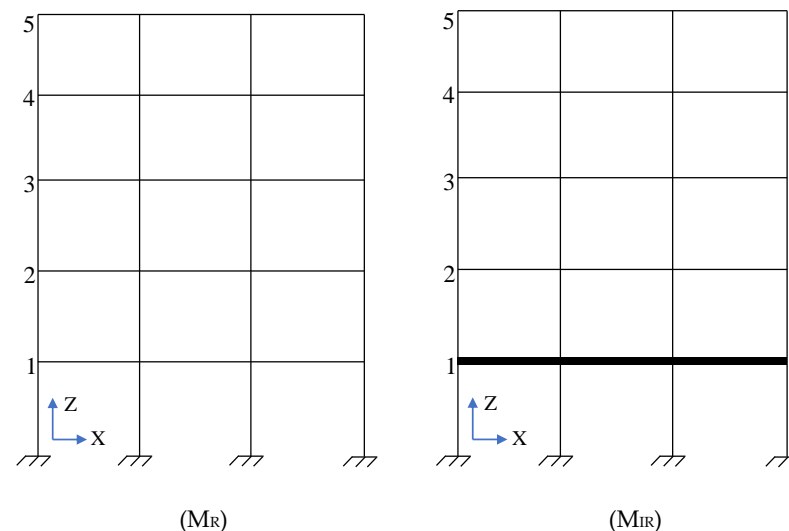

Figure 1. Elevation of five-story regular and irregular building models.

Frames have consistent beam sizes (300 mm × 450 mm) and column sizes (450 mm × 450 mm). The building frames are considered to be placed on three soil types (hard, medium, and soft). Each building frame was subjected to separate analysis for each soil type. To assess the seismic behavior of the building frames, the linear elastic response of bare frames was explored from the time history analysis using the Structural Analysis Program SAP2000 [32]. A Rayleigh damping model of 5% (associated with the first two modes in the 'X' direction) is defined to model the damping effects in the dynamic analyses. The ground motion selection approach employed in the current investigation is discussed in the next section.

3. Generation of FRS

The input load of an NSC to a major structure is typically calculated using the floor response spectrum. [15,16,33]. To the same extent as ground response spectra, floor response spectra define the most extreme characteristics of a floor's reaction to a motion. The dynamic interaction between the NSC and the main structure has always been ignored in calculations used to construct floor response spectra [5,33,34]. The floor responses are established once the primary structure is excited at its base. The corresponding floor response (floor acceleration time history) must be utilized to design the non-structural components. The steps involved in creating the FRS are depicted in Figure 2. The appropriate ground motion history is utilized as input for the primary structure analysis, as shown in Figure 2. The responses of the primary structure at the floor level, i.e., the acceleration history of the floor, are then input into an SDOF system to create FRS.
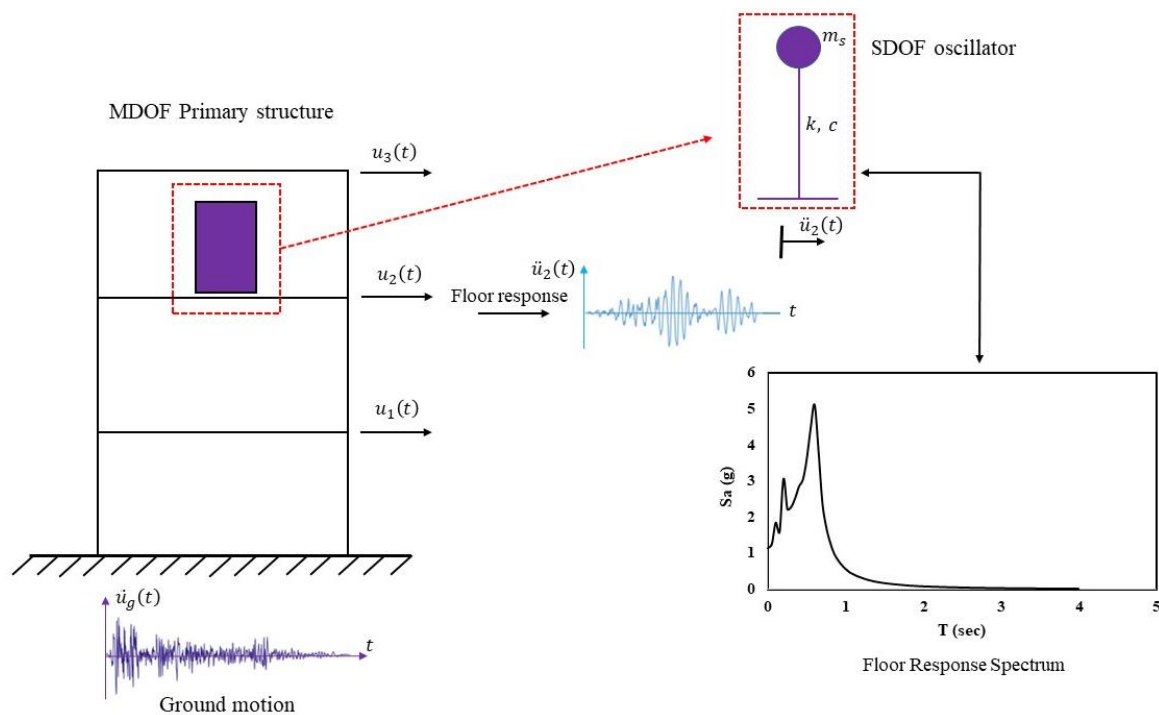
Figure 2. Generation of floor response spectrum.

4. Selection and Scaling of Ground Motions

In the seismic response assessment procedure, actual ground-motion records produce a realistic response [35,36]. The PEER [37] NGA-West2 Database has such records readily available. Hence, in the present study, 11 horizontal actual ground motion excitations were considered as per ASCE 7–16 [38] for each soil type. According to the NEHRP [39] site classification system, ground motions are selected based on shear wave velocity (V_{S30}) to represent hard, medium, and soft soils. The details of the excitations with respect to hard (Soil A), medium (Soil B), and soft soil (Soil C) are shown in Tables 1–3, respectively. Ground motions consistent with the design spectrum are chosen in this study because they can significantly save computing work [40]. The time-domain spectral matching approach suggested by [41] is used to produce spectrum-compatible earthquake excitations.

Table 1. Details of ground motions consistent with hard soil.

Earthquake	Year	Station	M_w	R_{jb} (km)	V_{s30} (m/s)
Helena_ Montana-01	1935	Carroll College	6	2.07	593.35
Helena_ Montana-02	1935	Helena Fed Bldg	6	2.09	551.82
Kern County	1952	Pasadena, CIT Athenaeum	7.36	122.65	415.13
Kern County	1952	Santa Barbara Courthouse	7.36	81.3	514.99
Kern County	1952	Taft Lincoln School	7.36	38.42	385.43
Southern Calif	1952	San Luis Obispo	6	73.35	493.5
Parkfield	1966	Cholame, Shandon Array #12	6.19	17.64	408.93
Parkfield	1966	San Luis Obispo	6.19	63.34	493.5
Parkfield	1966	Temblor pre-1969	6.19	15.96	527.92
Borrego Mtn	1968	Pasadena, CIT Athenaeum	6.63	207.14	415.13
Borrego Mtn	1968	San Onofre, So Cal Edison	6.63	129.11	442.88

Table 2. Details of ground motions consistent with medium soil.

Earthquake	Year	Station	M_w	R_{jb} (km)	V_{s30} (m/s)
Humbolt Bay	1937	Ferndale City Hall	5.8	71.28	219.31
Imperial Valley-01	1938	El Centro Array #9	5	32.44	213.44
Northwest Calif-01	1938	Ferndale City Hall	5.5	52.73	219.31
Imperial Valley-02	1940	El Centro Array #9	6.95	6.09	213.44
Northwest Calif-02	1941	Ferndale City Hall	6.6	91.15	219.31
Northern Calif-01	1941	Ferndale City Hall	6.4	44.52	219.31
Borrego	1942	El Centro Array #9	6.5	56.88	213.44
Imperial Valley-03	1951	El Centro Array #9	5.6	24.58	213.44
Northwest Calif-03	1951	Ferndale City Hall	5.8	53.73	219.31
Kern County	1952	LA, Hollywood Stor FF	7.36	114.62	316.46
Northern Calif-02	1952	Ferndale City Hall	5.2	42.69	219.31

Table 3. Details of ground motions consistent with soft soil.

Earthquake	Year	Station	M_w	R_{jb} (km)	V_{s30} (m/s)
Imperial Valley-06	1979	El Centro Array #3	6.53	10.79	162.94
Imperial Valley-07	1979	El Centro Array #3	5.01	14.54	162.94
Coalinga-01	1983	Parkfield, Cholame 2WA	6.36	43.83	173.02
Coalinga-01	1983	Parkfield, Fault Zone 1	6.36	41.04	178.27
Morgan Hill	1984	Foster City, APEEL 1	6.19	53.89	116.35
Superstition Hills-02	1987	Liquefaction Array	6.54	23.85	179
Superstition Hills-01	1987	Liquefaction Array	6.22	17.59	179
Whittier Narrows-01	1987	Carson, Water St	5.99	26.3	160.58
Loma Prieta	1989	Foster City, Menhaden Court	6.93	45.42	126.4
Loma Prieta	1989	Foster City, APEEL 1	6.93	43.77	116.35
Loma Prieta	1989	APEEL 2, Redwood City	6.93	43.06	133.11

SeismoMatch [42], a computer software, was used to spectrally match the ground motions to the target spectrum. SeismoMatch is an application that uses the wavelet approach to change earthquake ground motions and build a response spectrum almost identical to the target spectrum in a period range of interest. In this procedure, carefully selected basic wavelets are added and removed from the original record so that no further displacement is imposed. The essential properties of the original record in terms of the amplitude and frequency content of the record over the time history duration are retained, and the generated design time histories have spectra that are identical to the design spectra. Figure 3 shows the IS 1893:2016 target spectra associated with 5% damping and mean spectra of ground excitations for three different soil types. The average spectrum cannot be less than 90% of the target spectrum for the full period range, as stated in ASCE 7-16. From

the figure, it can be observed that the mean spectra are well above 90% of the target spectra in all soil types. Figure 4 shows the initial three linear modes, and Table 4 shows the first three modal periods of the considered building models. The mass participation ratios of structures are detailed in Table 5.
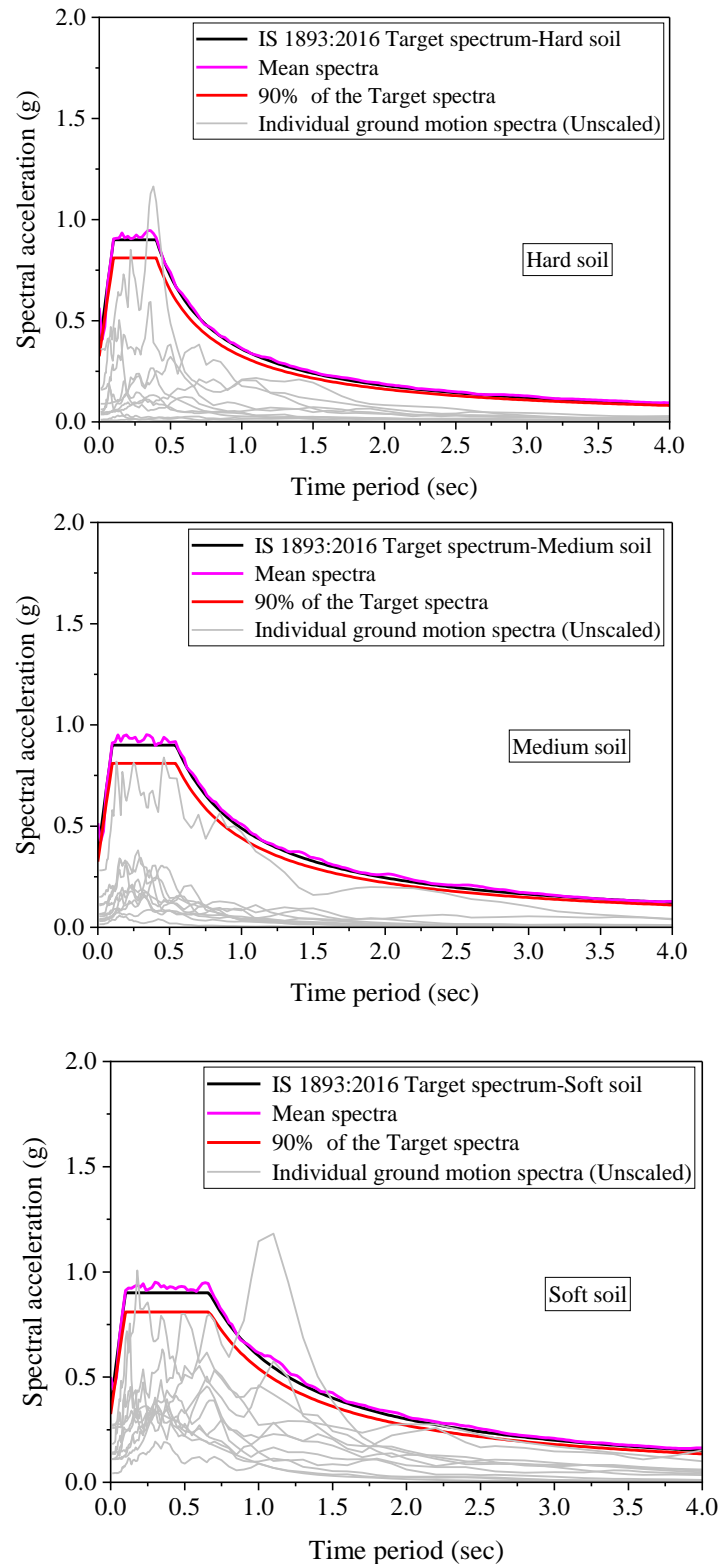

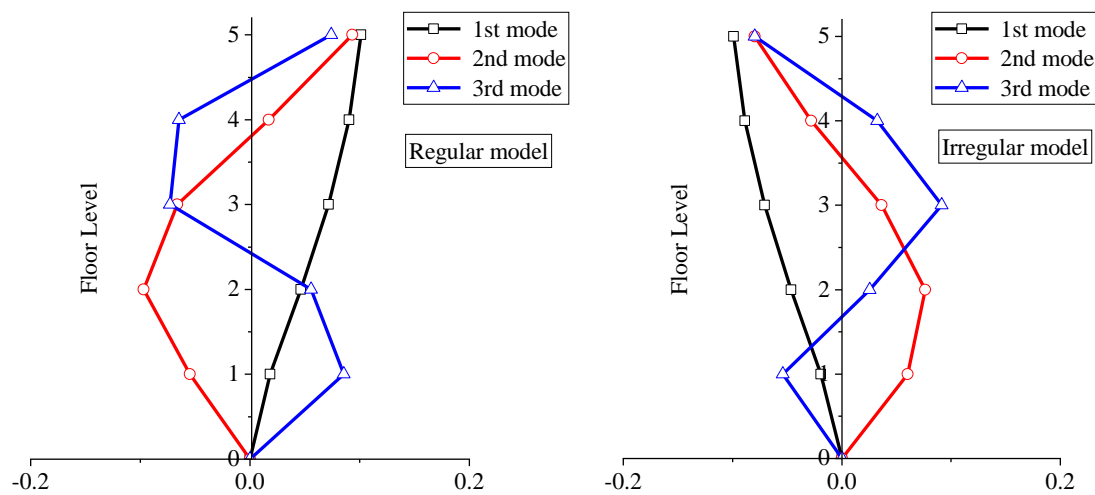**Figure 3.** Target and mean acceleration spectra for various soil types.

Figure 4. Mode shapes of regular and irregular building models.

Table 4. Modal periods (seconds) of the two building models.

	Regular Model	Irregular Model
1st mode	0.603	0.612
2nd mode	0.189	0.219
3rd mode	0.104	0.130

Table 5. Modal mass participation ratios of regular and irregular building models.

Mode	Regular Model		Irregular Model	
	UX	*UZ*	*UX*	*UZ*
1st	0.82	0	0.72	0
2nd	0.93	0	0.94	0
3rd	0.97	0	0.99	0
4th	0.99	0	1.0	0
5th	1.0	0.63	1.0	0.61
6th	1.0	0.63	1.0	0.61
7th	1.0	0.63	1.0	0.61
8th	1.0	0.86	1.0	0.83
9th	1.0	0.86	1.0	0.83
10th	1.0	0.93	1.0	0.93
11th	1.0	0.93	1.0	0.93
12th	1.0	0.96	1.0	0.96

5. Results and Discussion

5.1. Elastic FRS for Regular and Irregular Buildings

The mean response spectra were obtained from the floor response at various floor levels of two different building models. Floor response in the 'X' direction was calculated using a time history analysis of the building models for all three soil types by utilizing the ground excitations shown in Tables 1–3. The floor response obtained for each ground motion is sent into the SDOF system, which generates the floor response spectrum. The resulting individual response spectra are then used to calculate the mean floor response spectrum. The generated FRS is associated with the 5% damping ratio. Figures 5 and 6 show the elastic FRS for the regular and irregular buildings for all three soil types. Primarily, it can be observed from both figures that the response increases from the bottom first story to the top fifth story for all types of soils. Moreover, the figures show that the various peaks in the FRS correspond to the different fundamental modes of the building models. The peaks observed in the FRS are recorded close to elastic modal periods (Table 4). This

observation is consistent with the findings of the earlier study [14]. It has also been noted that mass irregularity (Figure 6) increases the floor spectral acceleration in all the floor levels for all soil types compared with the regular building model. It can also be inferred from the figures (Figures 5 and 6) that the floor spectral acceleration is observed to be more significant for soft soil (Soil C) than for medium and hard soils at all floor levels.
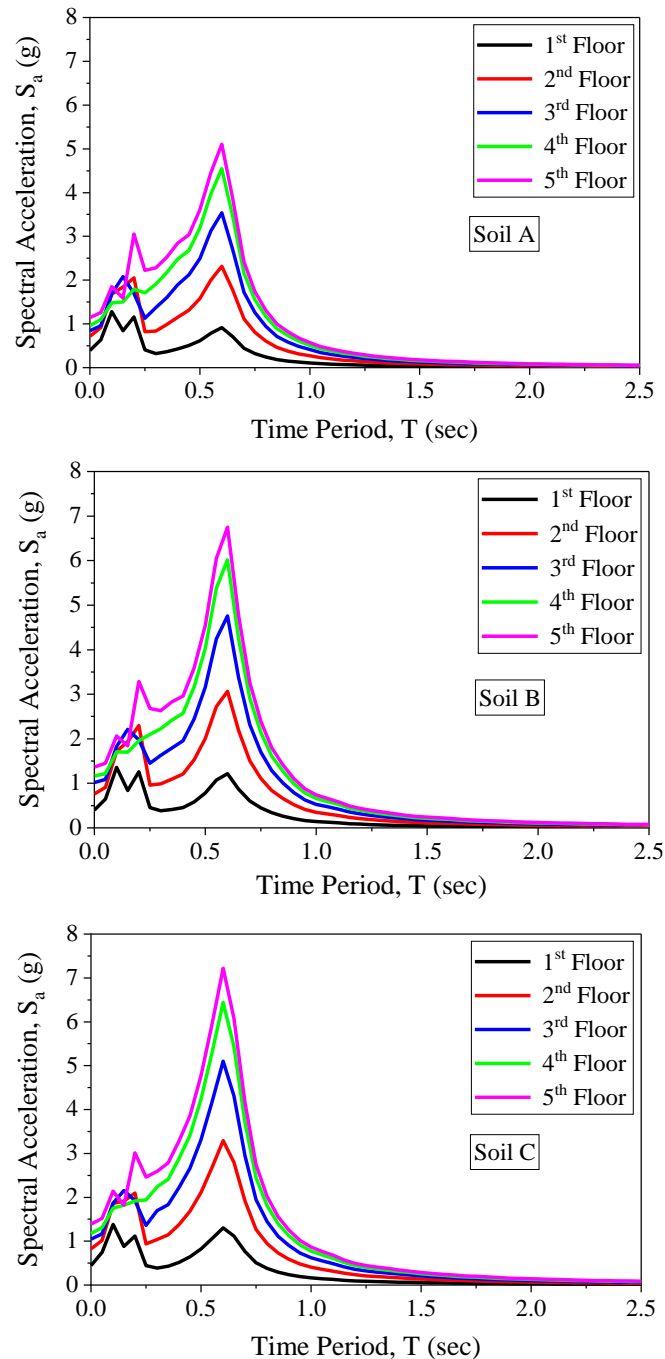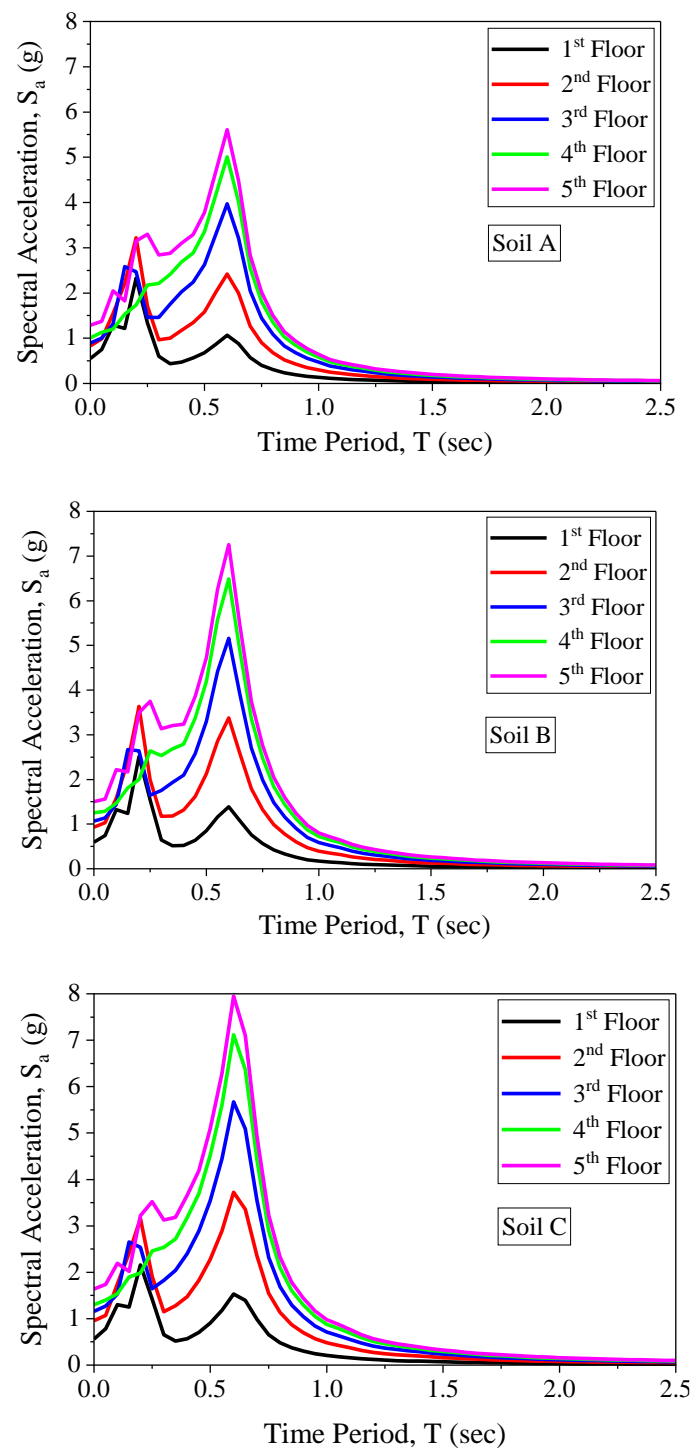
**Figure 5.** FRS of a regular building for various soil types.

Figure 6. FRS of an irregular building for various soil types.

In the FRS curves for the building models, the first, second, and third peak refers to the maximum response proximity to the first, second, and third modal periods, respectively. In the case of the M_R model (Figure 5), the first peak of spectral acceleration is the uppermost for the second, third, fourth, and fifth floor levels, whereas second and third peak floor spectral acceleration values are foremost for a lower story (first floor level). Similarly, for the M_{IR} model (Figure 6), two peaks are observed where the second peak acceleration value is the foremost for two floors (first and second floor levels), whereas the first peak response value is the uppermost for the remaining floor levels (third, fourth, and fifth). From Figures 5 and 6, it can be inferred that the spectral acceleration values increase with

soil flexibility. To better understand the effect of soil type on the FRS, the floor spectral acceleration of the building models with respect to the first modal period is shown in Figure 7. From the figure, the effect of soil type on the building models can be seen and is significant at higher floor levels. It can also be observed that the difference in the floor spectral acceleration between the medium and soft soil is less, whereas it is more between the hard and soft soil. The difference in the response between various soils increases with the floor level. Interestingly, under medium and soft soil, the floor spectral acceleration of a regular building rises by 32.4% and 41.3%, respectively, compared with the response under hard soil at the top level (5th floor). Compared with hard soil, the floor spectral acceleration of an irregular building at the highest floor level (5th floor) increases by 29.2% in medium soil and 41.5% in soft soil. Additionally, it can be shown that the irregular building exhibits an increase in floor response for hard soil of 26.1% and 10%, respectively, at the 1st and 5th floor levels, compared with the regular building. In medium soil conditions, the floor response increases in the irregular building by 14.04% and 7.5% at the 1st and 5th floor levels compared with the regular building. The floor spectral acceleration response increases in the irregular building by 17.7% and 10.12% at the 1st and 5th floor levels compared with the regular building for soft soil conditions. As a result, the existence of mass irregularity in the building frame has a substantial influence on the elastic building frame floor responses.
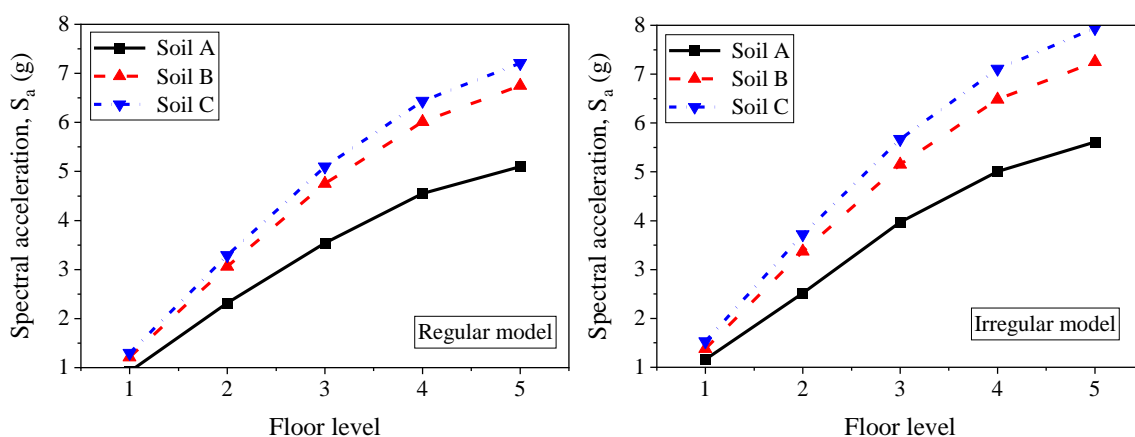
Figure 7. Peak floor spectral acceleration for different soil types with respect to 1st modal time period.

5.2. Normalized Floor Amplification

This research assesses a normalized floor amplification factor to examine the influence of irregularity on the floor response relative to the building's height (relative height is the ratio between the height of the structure with respect to the base and the height of the roof of the structure with respect to the base). Figure 8 shows the variation of peak floor response (PFR) normalized with a peak ground acceleration (PGA = 0.36 g) with the height of a building. This study considers the peak floor acceleration response as the PFR. It can be prudently observed from Figure 8a that the PFR/PGA values for regular buildings are 3.17, 3.79, and 3.85 on the 5th floor level for Soil A, Soil B, and Soil C conditions, respectively. At the same floor level, PFR/PGA values for irregular buildings (Figure 8b) are higher and are 3.60, 4.17, and 4.54 for Soil A, Soil B, and Soil C conditions, respectively.

Figure 9 compares the variation of the floor amplification for regular and irregular building models for different soil profiles. It is noted from Figure 9 that the ratio of PFR/PGA is larger for irregular buildings than regular buildings for all soil types. The floor acceleration is shown to be higher under soft soil (Soil C) conditions in both regular and irregular building models. It is clear from the figure that the values of the ratio PFR/PGA for all soil conditions range from 1.08 to 3.85 for regular buildings and 1.53 to 4.55 for irregular buildings. The variation of floor acceleration throughout the building height is found to be nonlinear irrespective of the type of building and the soil condition. A similar conclusion was derived with the help of a height factor in the study of Shang et al. [18].

Several code formulas exist to assess the variation of peak floor acceleration along with the structure's height. The floor amplification factor (*PFR/PGA*) specifications for several seismic codes, including ASCE 7-16 [38], Eurocode 8 [43], and GB 50011-2010 [44], are provided by Equations (1)–(3), respectively.

$$PFR/PGA = 1 + 2\frac{z}{h} \tag{1}$$

$$PFR/PGA = 1 + 1.5\frac{z}{h} \tag{2}$$
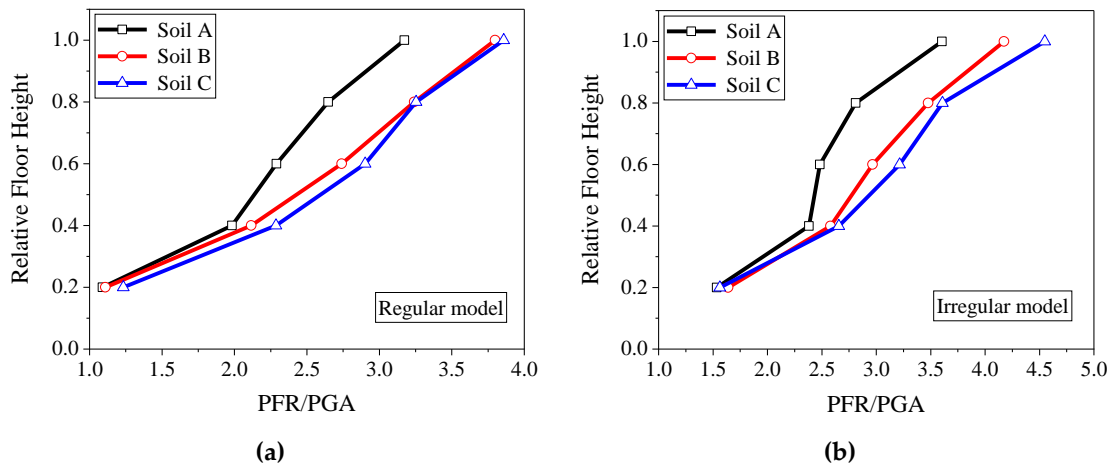
$$PFR/PGA = 1 + \frac{z}{h} \tag{3}$$

Figure 8. Normalized floor amplification of (**a**) regular building; (**b**) irregular building.
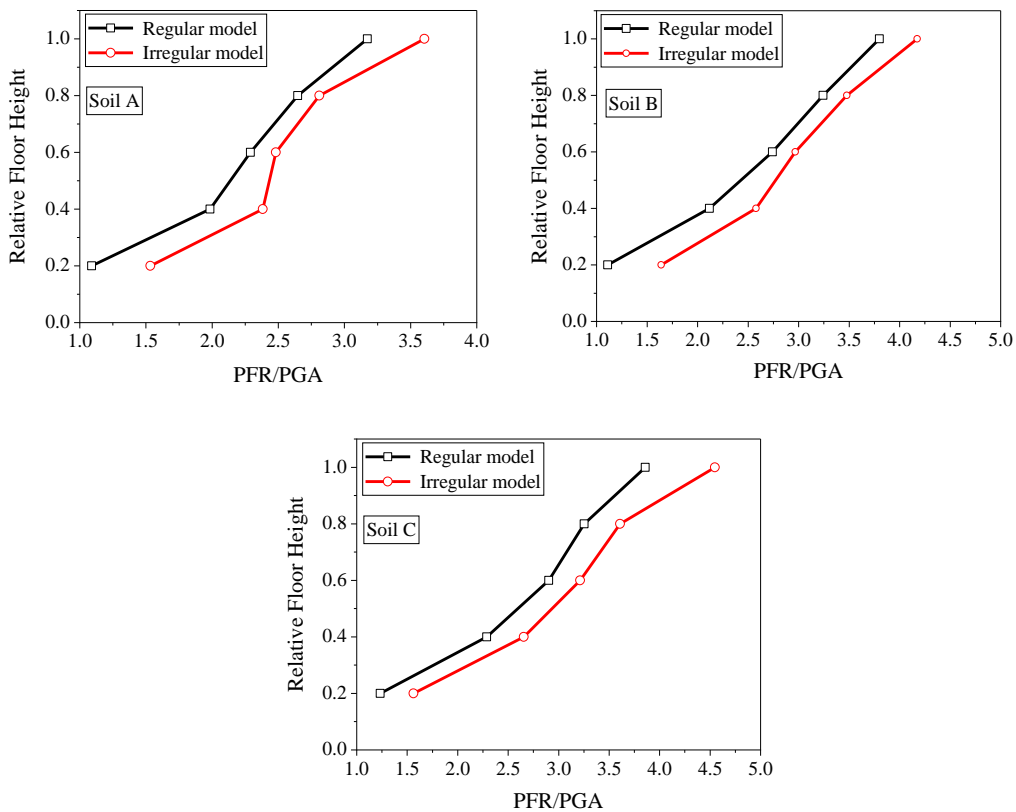

Figure 9. Comparison of normalized floor amplification between regular and irregular buildings for different soil types.

From Figure 10, it can be observed that ASCE 7-16 overestimates the PFR demands for a regular model and underestimates those for an irregular model at a lower story (first floor level) in all soil types. ASCE 7-16 underestimated the PFR demands in regular and irregular building models for the remaining floor levels. Eurocode 8 and GB 50011 also underestimated the PFR demands in regular and irregular building models along with the height of the building except at the first floor level. Figure 11 compares the floor amplification factors acquired in this study with those derived from the formulation suggested by the Applied Technology Council (ATC) in the USA. This formulation can be seen in Equations (4)–(7).

$$PFR/PGA = 1 + a_1 \left[\frac{z}{h}\right] + a_2 \left[\frac{z}{h}\right]^{10} \tag{4}$$

$$a_1 = \frac{1}{T_{abldg}} \leq 2.5 \tag{5}$$

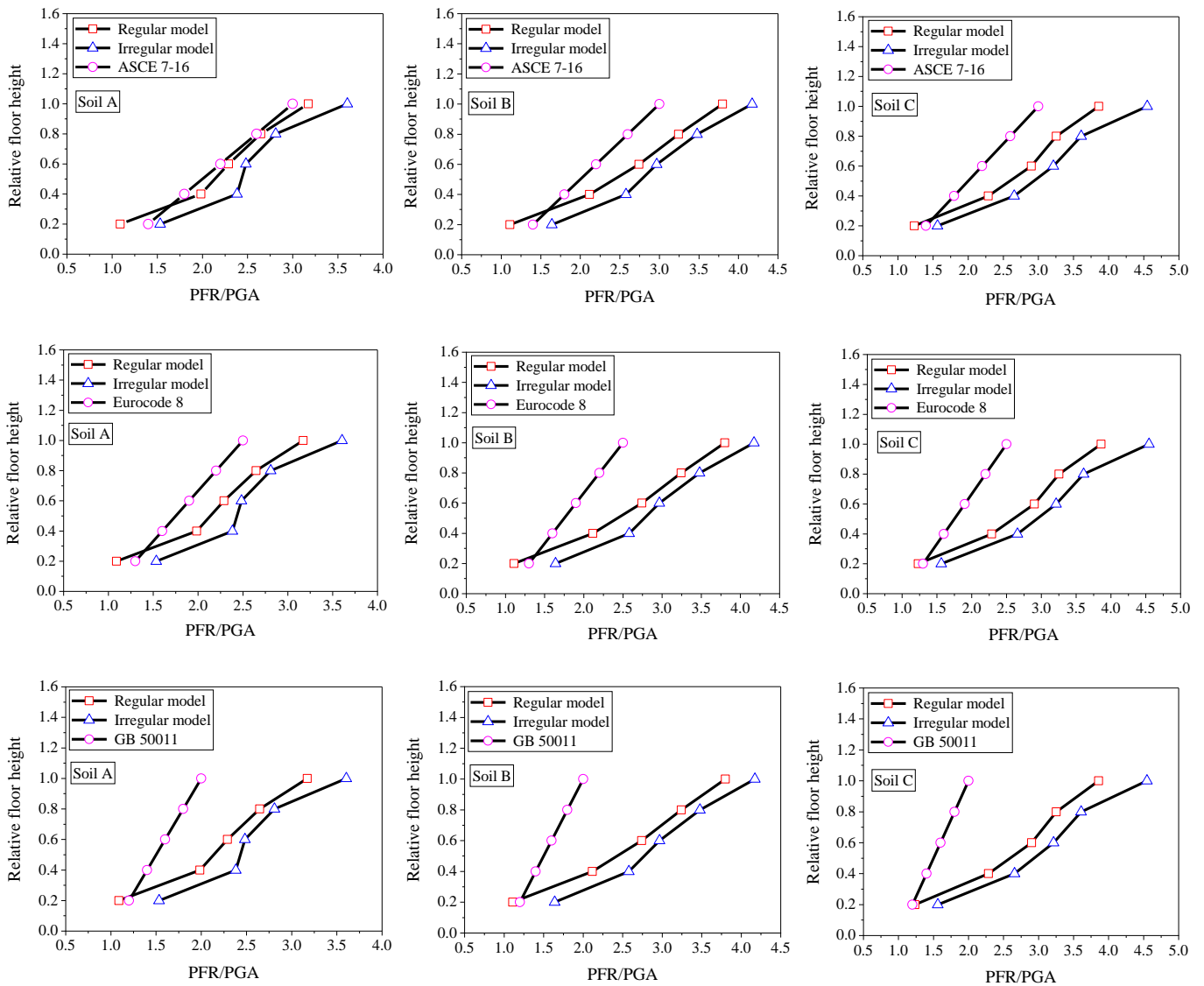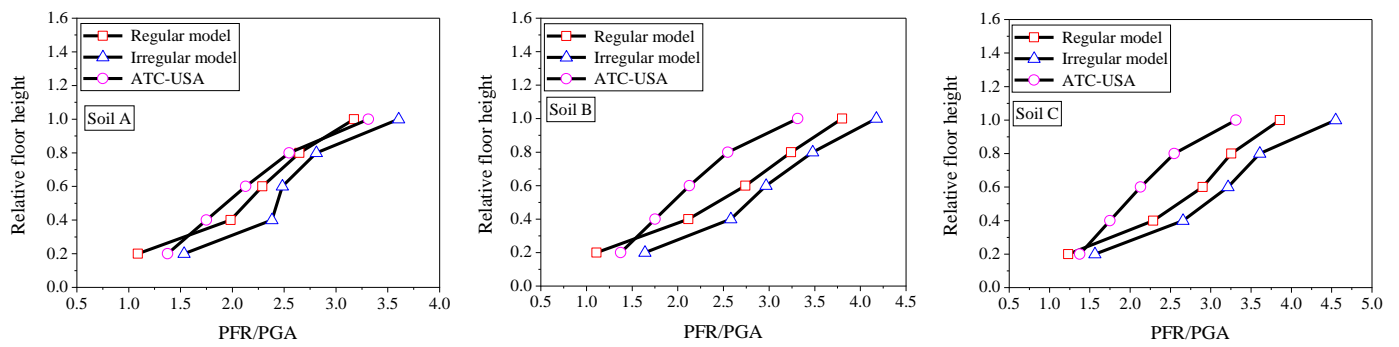$$a_2 = \left[1 - \left(\frac{0.4}{T_{abldg}}\right)^2\right] > 0 \tag{6}$$

Figure 10. Comparison of floor amplification factors between the considered building models and current codes.

Figure 11. Comparison of floor amplification factors between the considered building models and ATC-USA.

According to ASCE/SEI 7-16 [38] equation 12.8–7, T_{abldg}, also known as the estimated fundamental translational period of the building, is as follows:

$$T_{abldg} = C_t h_n^x \tag{7}$$

where h_n is the height of the building in meters, and the coefficients C_t and x are determined from Table 12.8–2 of ASCE/SEI 7-16 [38].

From the ATC-USA formulation, it can be inferred that the floor amplification factor depends on the fundamental period of the building. It is noted from the figure (Figure 11) that the PFR/PGA values from the ATC formulation correlate well with the values from the regular model for soil A. It underestimates the PFR demands of an irregular model in soil A and regular and irregular models in soil B and C conditions. Therefore, it can be inferred that the linear hypothesis in the code-based formulae may result in an under- or overestimation of PFR demands. The current code-based formulae may be modified by incorporating the effects of soil type and structural irregularity in the analysis, as their effect can be seen on the PFR demands. In light of this, it can be said that the code-based relationships do not adequately estimate the peak response of non-structural components together with building height.
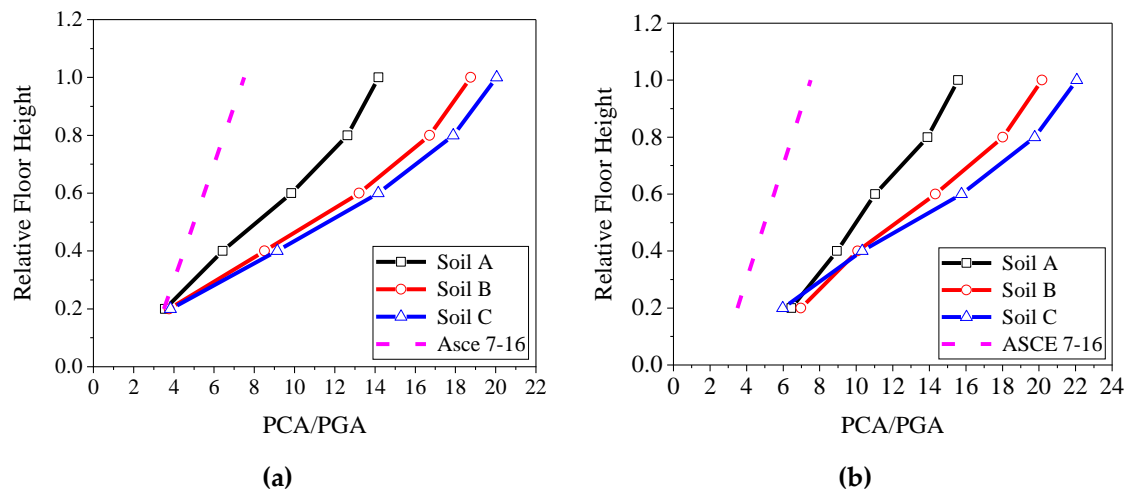
5.3. Peak Component Acceleration

The highest ordinate value in the floor response spectrum (FRS) is the peak component acceleration (PCA). The ASCE/SEI 7-16 gives the equation for a normalized PCA to the PGA (PCA/PGA) as defined in Equation (8):

$$PCA/PGA = a_p \left(1 + 2\frac{z}{h} \right) \tag{8}$$

where a_p is the dynamic amplification factor of a component equal to 2.5 for flexible NSCs and 1.0 for rigid NSCs. The variation of PCA/PGA values along with the relative floor height (z/h) is shown in Figure 12 for both regular and irregular building models for different soil types.

From Figure 12, it can be observed that the values of the PCA response were found to be more significant for irregular buildings under all soil conditions. The soil type shows a significant effect on the PCA response, and the corresponding values were larger for soft soil (soil C) when compared with the other two soil types, especially at the top story level. It can also be observed that the formulation given by ASCE 7-16 underestimates the PCA response along the building height. The ASCE formulation underestimates the PCA response by 89%, 150%, and 167% for a regular building model, and by 107%, 169%, and 194% for an irregular building model for soil types A, B, and C, respectively, at the top story level. From this analysis, it can be concluded that the code-based linear formulation cannot accurately estimate the peak acceleration response of the NSCs.

Figure 12. Normalized PCA values for (**a**) regular buildings; (**b**) irregular buildings.

5.4. Component Dynamic Amplification Factor

This section investigates the amplification in the acceleration of the component relative to the floor acceleration to which it is attached. The top-story FRSs of a regular and irregular building model under different soil types normalized by the corresponding peak floor accelerations (PFAs) are shown in Figure 13. The ratio of FRS to the PFA is known as a component dynamic amplification factor (CDAF). The CDAF of the building models in the present study is compared with the definitions of ASCE 7-16 [38] and FEMA P-750 [39]. As per the definition of ASCE 7-16, the component amplification factor is 2.5 for flexible NSCs whose time period is larger than 0.06 sec. For rigid NSCs ($T < 0.06$ s), the value of the amplification factor is 1. From Figure 13, it is clear that the definition of ASCE 7 underestimates the CDAF for periods closer to the vibration periods of the regular and irregular building models for hard soil, while it underestimates the CDAF for a period closer to the fundamental vibration period of the building models for medium and soft soil conditions. The maximum amplification factors for the top story of a regular building model are 4.47, 4.93, and 5.19 for soil A, B, and C, respectively. The corresponding values for an irregular building are 4.32, 4.83, and 4.85 for soil A, B, and C, respectively. As shown in Figure 13, this underestimation is also included in the definitions of FEMA P-750.

The effect of the damping ratio of NSC (ξ_{NS}) on the seismic behavior of non-structural components must be assessed, as NSCs are characterized by different periods and damping ratios [45]. Hence, in this particular study, component dynamic amplification factors are evaluated for different ξ_{NS} (0.1%, 0.2%, 0.5%, 1%, 2%, 5%, 10%, and 20%). Figure 14 shows the top floor CDAF spectrum of regular and irregular building models for different NSC damping ratios (0.5%, 2%, and 10%). Lower ξ_{NS} values resulted in higher amplification factor values, as expected. The effect of the damping ratio of NSC is found to be more significant at modal periods of the building models for all soil types. It is worth noting that the effect of ξ_{NS} is insignificant over both very short and very long periods. As a result, this study attempted to develop a CDAF spectrum prediction model using one of the machine learning techniques known as artificial neural networks (ANNs).
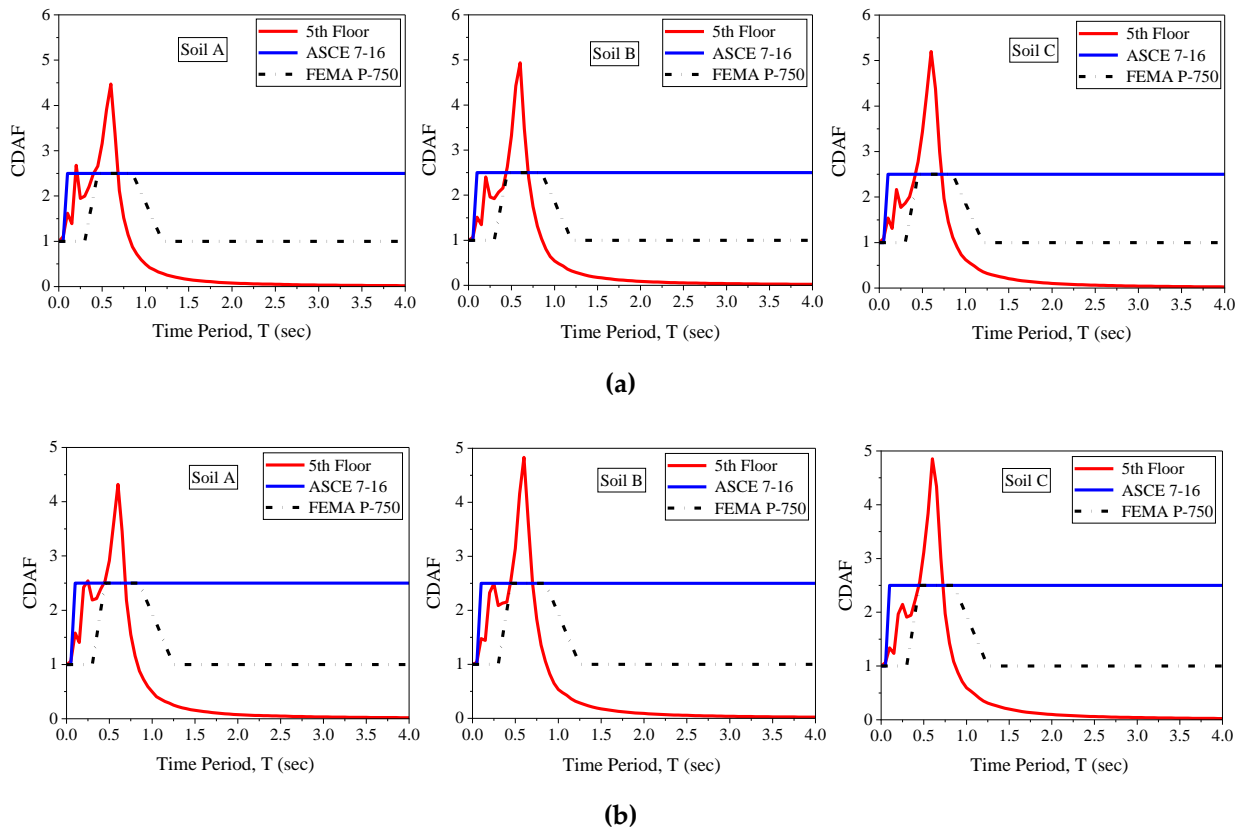
Figure 13. CDAF for a top floor level (**a**) regular building; (**b**) irregular building.
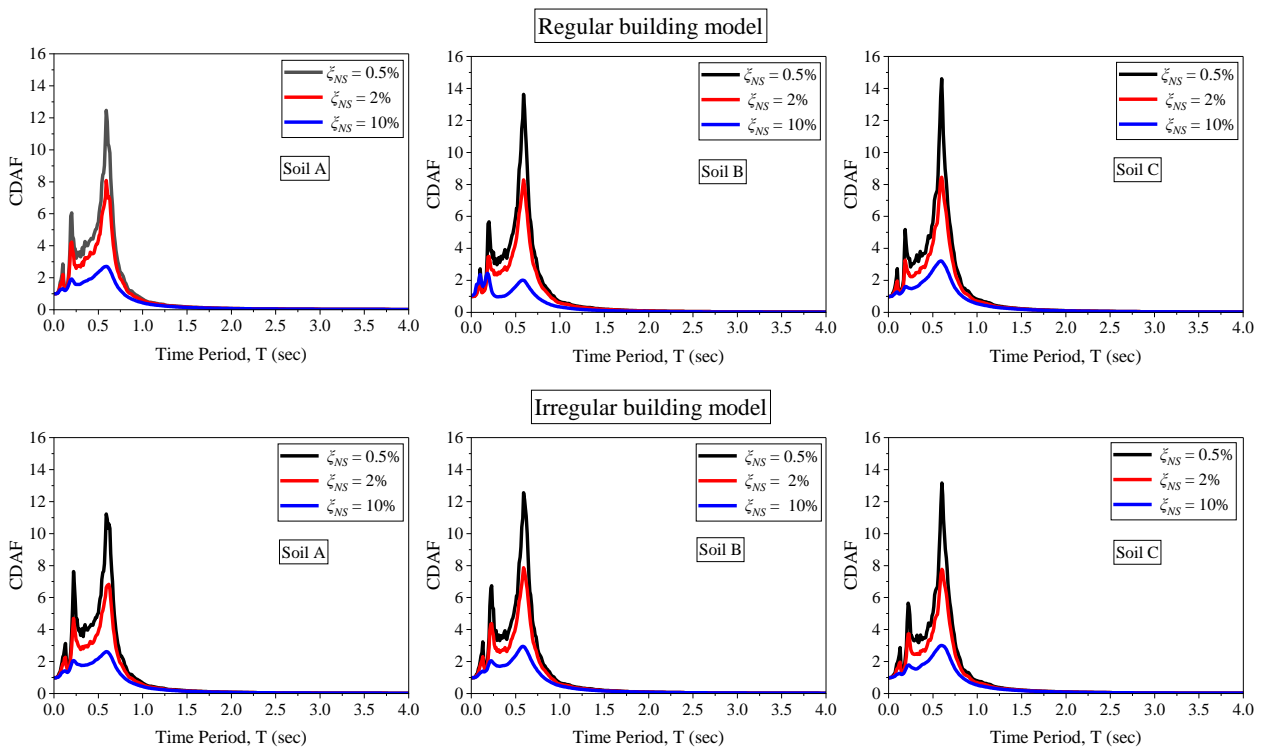

Figure 14. CDAF spectrum for a top floor at various damping ratios of NSC.

6. Artificial Neural Network (ANN) Model

Artificial neural networks (ANNs) are assisting in the resolution of a wide range of engineering issues [46,47]. ANNs are expressed mathematically as a simplified model analogous to biological neural networks. Neural networks can evaluate enormous volumes of data and deal with complex and confusing situations. As a result, neural networks are often a better calculation and prediction tool than classic computation approaches [48]. Researchers all over the globe have effectively employed neural networks in the subject of structural dynamics [8,49–51]. Hence, in this study, a feed-forward neural network with two layers is used to predict the CDAF spectrum accurately. The hidden layer is one of two layers, the other being the output layer. Neural networks with only one hidden layer may precisely approximate any function [52]. The vibration period (T = 0 to 2 s with 0.01 interval) and damping ratio (ξ_{NS}) of the NSC, soil type (S), where S = 0, 1, and 2 for Soil A, B, and C, respectively, and floor level are considered as inputs for the model. The CDAF values represent the model's expected output. The network's architecture has a more significant influence on the model's performance. The optimum number of hidden neurons is identified based on the minimum MSE (mean squared error) of the output. The MSE is defined as per Equation (9) as follows:

$$MSE = \frac{\sum (Y_s - Y_p)^2}{n} \tag{9}$$

where Y_s and Y_p are the simulated and predicted outputs, and n is the number of data points. Figure 15 shows the variation of MSE with the number of hidden neurons. The figure shows that the lowest MSE is attained with 17 hidden neurons. Thus, the ANN 4-17-1 model (Figure 16) was developed by taking into consideration the 17 neurons in the hidden layer.

A suitable learning strategy must be developed to train the hidden neurons. The Levenberg–Marquardt (LM) back propagation (BP) technique is used to train the network. Furthermore, the Tan-sigmoid transfer function is used in both the hidden and output layers. The neural network model in this study was created on the MATLAB R2019b environment. In total, 24120 CDAF values were simulated for each building model in this study corresponding to 201 vibration periods of NSC, 8 damping ratios, 3 soil types, and 5 floor levels. The dataset is further randomly subdivided into 3 sections: training (70% of the total dataset), validation (15% of the total dataset), and testing (15% of the total dataset). Before training, the entire dataset must be preprocessed. The dataset must be normalized between -1.0 and 1.0 in order to provide equal weightage to the variables. This normalization can be conducted using Equation (10):

$$X_n = \frac{2(X - X_{min})}{(X_{max} - X_{min})} - 1 \tag{10}$$

where X_n is the normalized value, and X_{max} and X_{min} are the maximum and minimum values of the variable X. The prediction capability of the ANN model is evaluated by defining the performance measurement functions. The coefficient of correlation (R) and mean square error (Equation (9)) are two performance measuring functions used in this study. The following is a definition of the coefficient of correlation (Equation (11)):

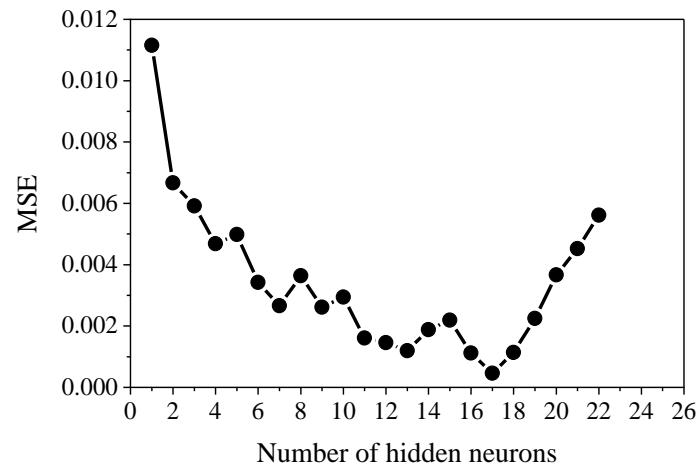$$R = \sqrt{\frac{\sum Y_s^2 - \sum (Y_s - Y_p)^2}{\sum Y_s^2}} \tag{11}$$

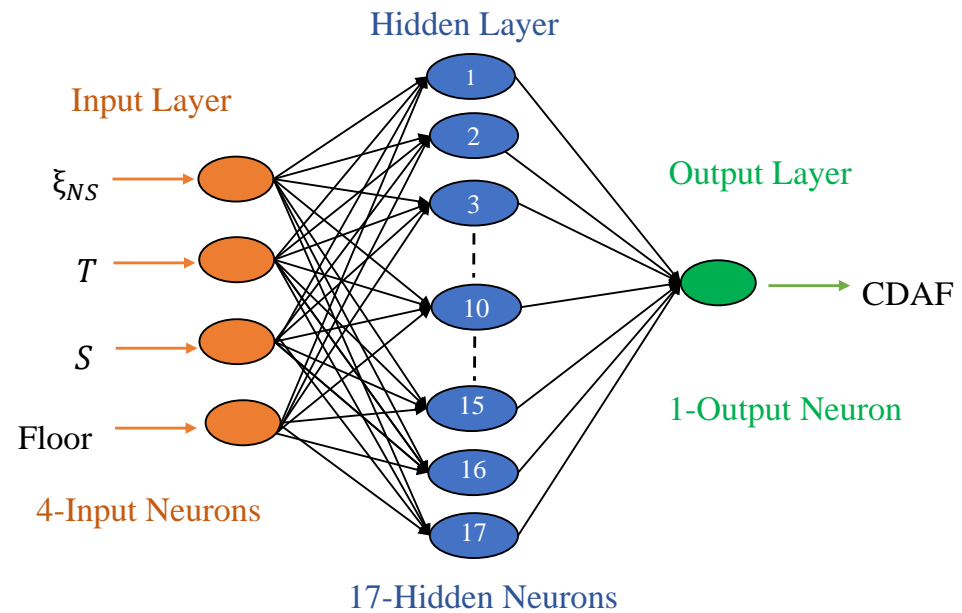**Figure 15.** Variation of *MSE* with the number of hidden neurons.

Figure 16. ANN 4-17-1 model.

The results of the model's performance are shown in Table 6. The *R* value should be as high as possible, and the error (*MSE*) should be minimal. Figures 17 and 18 show the correlation between the simulated and predicted CDAF of regular and irregular building models. These figures show that all simulated data points are close to the 45-degree line. The 45-degree line represents the residual-free line (i.e., predicted data = simulated data). The predicted data are obtained by the prediction model (ANN), whereas the simulated data are generated using the approach described in Section 5.4. The points should be on the 45-degree line if the model delivers extremely accurate predictions. Otherwise, the points are spread out along that line. The correlation coefficient is near to unity, indicating that the model well predicts the component dynamic amplification factor values.
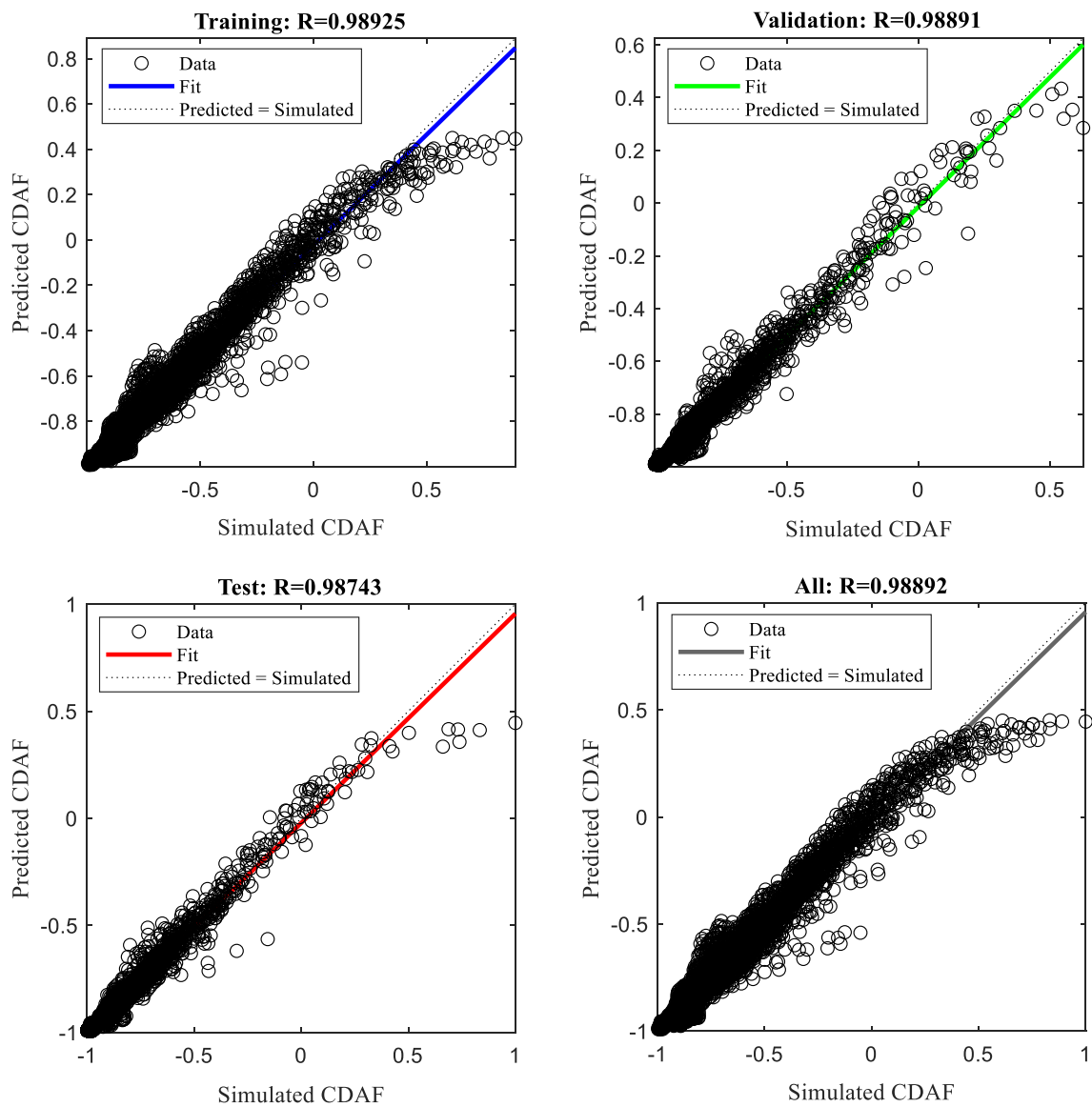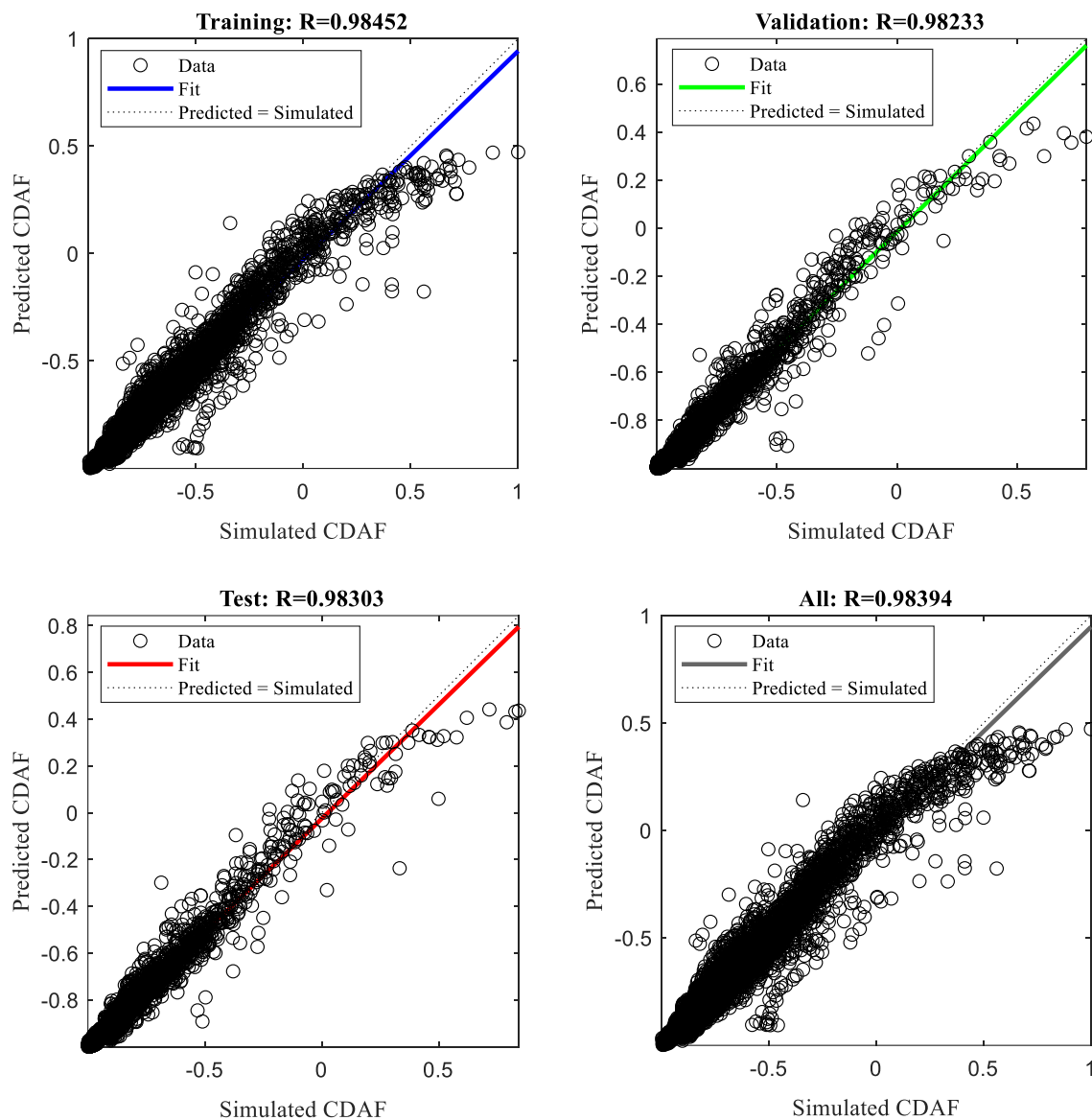
Figure 17. Simulated and ANN's predicted CDAF for a regular building model.

Table 6. Performance of ANN model.

Dataset	Regular Model		Irregular Model	
	R	*MSE*	*R*	*MSE*
Training	0.989	0.00091	0.984	0.0012
Testing	0.987	0.00096	0.983	0.0019

Figure 18. Simulated and ANN's predicted CDAF for an irregular building model.

6.1. Predictive Expression Using ANN Model

In this section, the relationship between the inputs and output is developed. The weights and bias values between the inputs and output from the trained ANN models are utilized to develop the predictive expressions. Prior research has demonstrated the value of such expressions, and built comparable prediction correlations for various problems [8,51,53,54]. Tables 7 and 8 provide the weights and biases of the ANN model for regular and irregular building models, respectively.

Table 7. Weights and biases of the ANN model for regular building.

Hidden Neuron	Input-Hidden Weight				Hidden-Output Weight	Bias	
	T	ξ_{NS}	S	Floor	CDAF	Hidden	Output
1	−68.809	−3.090	46.460	−4.962	−0.143	−8.113	
2	3.427	0.113	−0.063	−0.021	−1.425	0.611	
3	−68.642	−6.979	11.368	0.189	0.053	−34.320	
4	0.137	4.842	0.009	0.019	−13.283	7.106	
5	22.380	0.396	8.460	1.107	0.130	11.461	
6	−5.362	−0.109	4.665	−1.013	4.460	−3.463	
7	−32.567	−1.630	28.505	27.228	0.044	25.297	
8	−17.193	−0.253	0.019	−0.010	14.987	−7.060	
9	17.085	0.202	−0.018	0.015	15.110	7.019	10.732
10	34.729	0.493	0.056	−1.679	0.370	31.978	
11	5.423	0.078	−4.727	1.190	−8.203	4.012	
12	−2.685	0.239	−0.038	1.322	−0.239	−2.188	
13	−5.118	−0.085	4.431	−1.058	−12.737	−3.639	
14	2.966	0.081	0.020	0.519	0.976	2.195	
15	−46.845	−43.367	−0.059	0.496	0.078	−60.467	
16	−33.267	−0.202	−0.096	−0.223	−11.119	−27.673	
17	30.736	0.220	0.099	0.261	−11.738	25.571	

Table 8. Weights and biases of the ANN model for irregular building.

Hidden Neuron	Input-Hidden Weight				Hidden-Output Weight	Bias	
	T	ξ_{NS}	S	Floor	CDAF	Hidden	Output
1	−1.823	−7.929	−0.136	0.233	−2.726	4.917	
2	1.926	13.893	0.032	−0.192	1.251	3.018	
3	−1.796	0.169	0.061	−0.003	2.886	0.085	
4	−5.367	−0.440	−6.494	2.704	0.118	−1.311	
5	−6.863	6.238	0.071	−0.298	2.718	2.136	
6	−6.562	5.712	0.081	−0.301	−2.957	1.885	
7	8.947	−1.633	0.050	7.035	−0.100	−3.219	
8	20.749	2.468	0.057	−0.922	0.482	20.907	
9	26.644	0.166	0.027	0.403	−4.378	21.303	−3.109
10	−14.638	0.262	0.007	−0.020	−8.095	−5.555	
11	0.157	4.150	0.014	−0.001	1.447	3.074	
12	7.773	0.332	11.839	−7.140	−0.103	13.698	
13	−14.563	0.188	0.010	−0.012	8.206	−5.490	
14	−36.300	−1.397	0.126	−3.951	−0.289	−26.922	
15	32.328	0.135	0.024	0.279	3.800	25.904	
16	−0.177	0.404	−0.010	−0.005	−14.903	−0.063	
17	3.627	−0.032	1.161	−2.418	−0.157	−1.237	

By inserting the weights and biases (Tables 7 and 8) into Equation (12) [8], the predictive expression for $CDAF$ can be developed. The procedure explained in the reference study [8] to develop a predictive expression (normalized) was followed precisely in the current study to establish a proper relationship between the inputs and outputs. The resultant denormalized predictive expressions for $CDAF$ are as shown in Equations (13) and (14) for regular and irregular building models, respectively:

$$Y_n = f_o\left\{b_o + \sum_{k=1}^{h}\left[w_k \times f_h\left(b_{hk} + \sum_{i=1}^{m}w_{ik}X_{ni}\right)\right]\right\} \qquad (12)$$

where b_o = bias of the output layer; w_k = weight connection between hidden layer neuron (k) and single output neuron; b_{hk} = kth hidden neuron bias; w_{ik} = weight between the input and hidden layer neuron (k); X_{ni} = input parameter; f_h = transfer function of the hidden layer (Tan-sigmoid); and f_o = transfer function of the output layer (Tan-sigmoid):

$$CDAF_{regular} = \left(10.25 \times CDAF_{n,regular}\right) + 10.29 \tag{13}$$

$$CDAF_{irregular} = \left(9.735 \times CDAF_{n,irregular}\right) + 9.7691 \tag{14}$$

where $CDAF_{n,regular}$ and $CDAF_{n,irregular}$ are the normalized component dynamic amplification factors of regular and irregular building models, respectively. Only the dataset range for which the ANN model was developed should be utilized in Equations (13) and (14). The maximum and minimum input parameter constraints are shown in Table 9.

**Table 9.** Limits of input and output parameters.

	Input Parameters				Output Parameter	
					CDAF	
	T (sec)	ζ_{NS} (%)	S	Floor	Regular Model	Irregular Model
Max	2	20	2	5	20.545	19.504
Min	0	0.1	0	1	0.038	0.034

6.2. Validation of ANN-Based Predictive Expression

This study attempted to assess the applicability of the ANN model/s in forecasting the dynamic amplification factors of non-structural components attached to the regular and irregular building models for different soil types. For such validation, the CDAF spectra of the top floor (5th floor) of the considered building models were generated for all soil types by considering 0.7% and 3% as the damping ratios of NSC. The considered damping ratio values for the validation were not utilized in developing ANN prediction models. Figure 19 shows the simulated and predicted CDAF spectra for regular and irregular building models. It can be seen that there is relatively excellent agreement between the predicted and simulated spectra for all the investigated cases.


Figure 19. *Cont.*

(a)

(b)
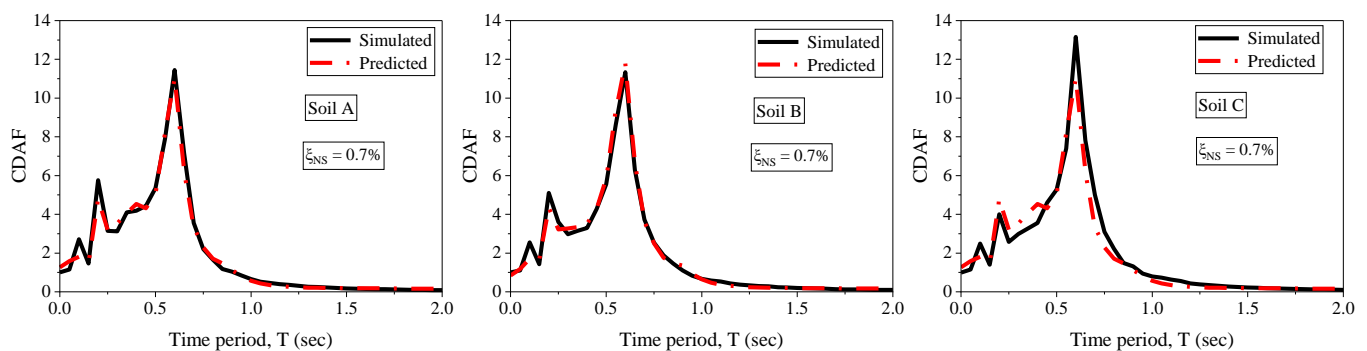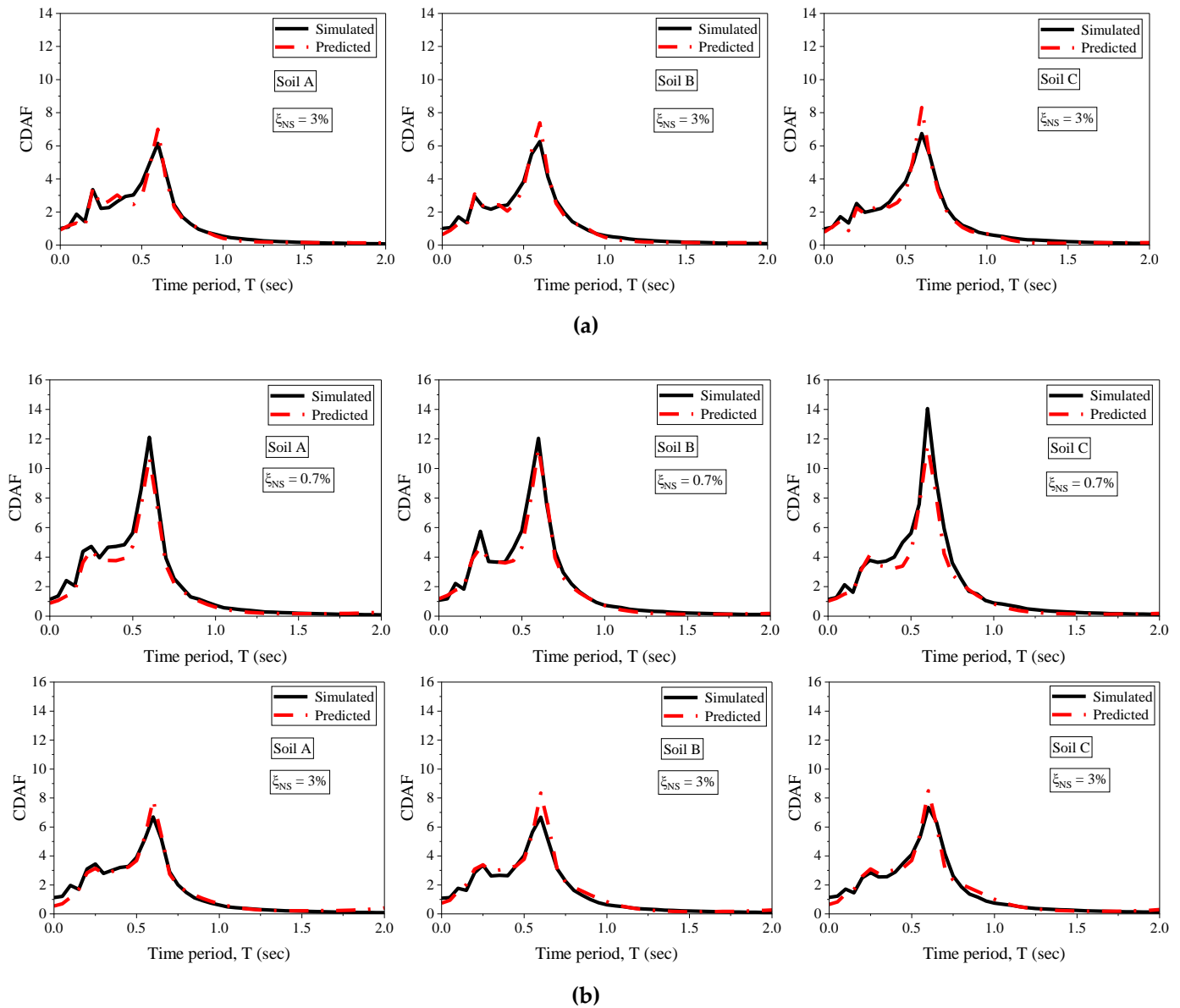
Figure 19. Top floor simulated and ANN's predicted CDAF spectra: (**a**) regular model; (**b**) irregular model.

Furthermore, the efficiency of the ANN models was verified by comparing the amplification factors obtained in this study with those obtained from the formulation given in the reference study [18] which is defined as shown in Equation (15) [18]:

$$\text{Amplification factor} = 30.136 \times (1 + \xi_{NS})^{-0.864} \tag{15}$$

The amplification factor is defined as the maximum value of the CDAF described in the previous sections. Figure 20 shows the comparison of amplification factors of the top floor of the considered building models for all soil types by the proposed ANN models of Equations (13) and (14) with those obtained from Equation (15) [18]. It is clear from Figure 20 that the variation of predicted amplification factors with damping ratio follows the same pattern as that of the existing formulation of Ref. [18]. The slight difference between them is due to the difference in considered building models, ground motions, target spectrum, and soil type. However, the proposed formulation of Equations (13) and (14) closely relates to the existing formulation for soil type C (soft soil). This is because the existing formulation in the reference study [18] was developed by considering the soft

soil (Type III) as per the Chinese seismic design code [44]. Therefore, the proposed ANN models of Equations (13) and (14) can effectively estimate the seismic demands of NSC for all soil types.
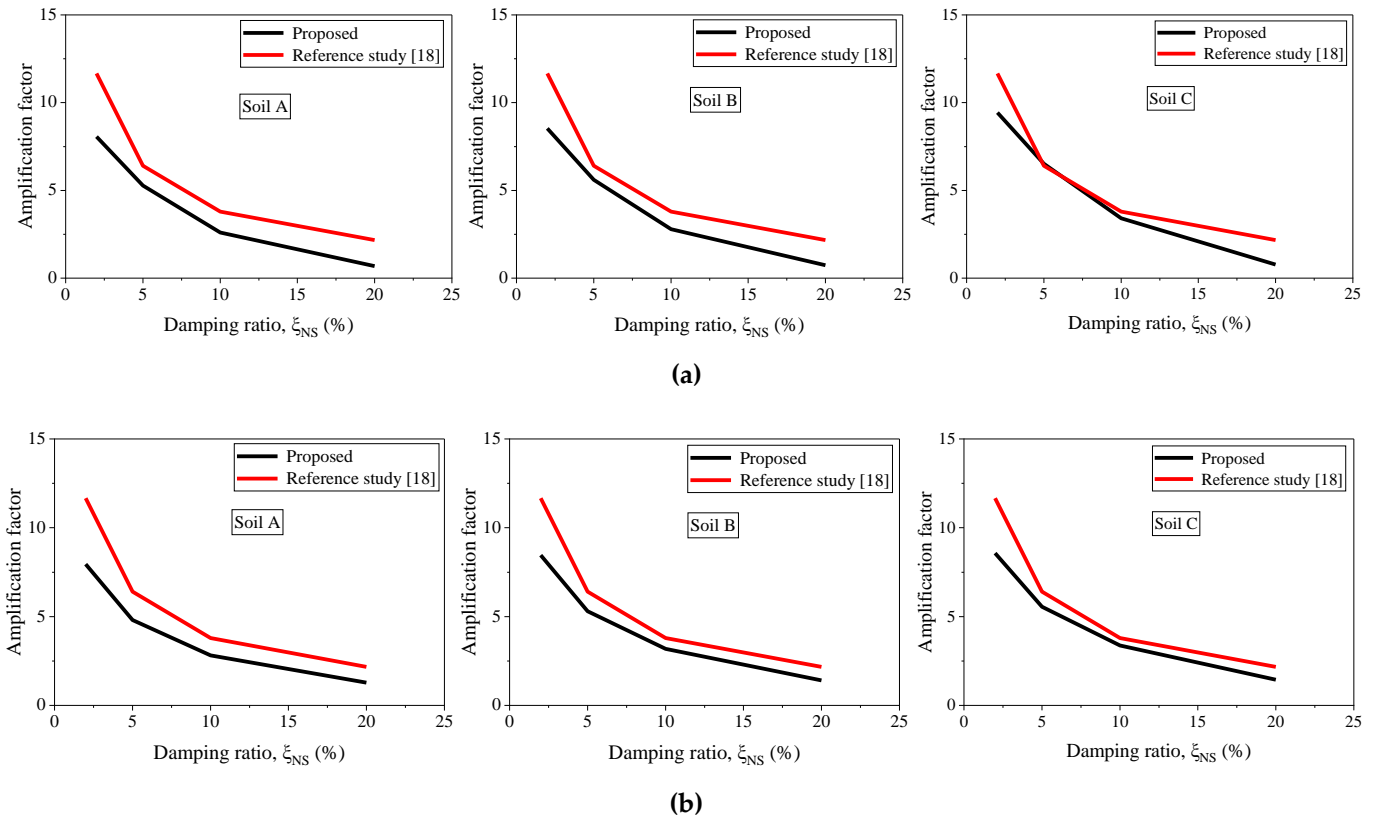
Figure 20. Comparison of amplification factors: (**a**) regular model; (**b**) irregular model.

7. Summary and Conclusions

Non-structural components (NSCs) have become critical in sustaining post-earthquake functionality while constructing seismic-resilient structures. Floor response spectra can be used to measure the seismic load on non-structural components. The present study was dedicated to assessing the seismic demands on NSC via FRS. The NSCs studied are single degree of freedom structures. The building structures considered are five-story regular and irregular reinforced concrete framed structures. The mass irregularity was considered at the first story level in the case of an irregular building as per the requirement of IS 1893:2016 (Part 1). The major goal of this research was to examine how different soil types affect the seismic response of NSCs. According to the IS 1893 code, three types of soil are considered: soil A, soil B, and soil C. For the time history analysis, 11 ground motions for each soil type were considered and they were made compatible with the IS code-based design spectrum. The building structures were subjected to those 11 numbers of spectrally matched ground motions for each soil type. The response of the regular and irregular structures on each floor is calculated for different soil types and spectrally matched ground motions. The mean floor response spectra were constructed from the floor responses at each floor level. Based on the analysis of the building models, the following conclusions are drawn:

- The peaks observed in the floor response spectra correspond to the fundamental natural periods of the considered building models.
- The presence of mass irregularity at the lower story of the considered building models amplified the floor acceleration response at all floor levels for all soil types.
- Floor acceleration response increased in the irregular building by 26.1% and 10% at 1st and 5th floor levels for hard soil compared with the regular building.

- Floor spectral acceleration values increase with an increase in soil flexibility. In comparison with the hard soil, the floor spectral acceleration of a regular building's 5th story increases by 32.4% in medium soil and by 41.3% in soft soil. Similarly, the floor spectral acceleration of an irregular building at the highest floor level (5th floor) increases by 29.2% in medium soil and 41.5% in soft soil compared with hard soil.
- Independent of building and soil type, it is found that the floor acceleration varies nonlinearly with building height. The values of the floor amplification factor increase with the building height and range from 1.08 to 3.85 for regular buildings and 1.53 to 4.55 for irregular buildings.
- The linear assumption in the code-based floor amplification formulation may lead to overestimation (first floor) and underestimation (second to fifth floor) of peak floor response demands.
- The code definitions underestimate the peak component acceleration and dynamic amplification factors for all soil types.
- The code definitions underestimate the CDAF for non-structural component periods closer to the vibration periods of the regular and irregular buildings for hard soil, while for medium and soft soil types, code definitions underestimate the CDAF for a non-structural component period closer to the fundamental vibration period of the building.
- The 4-17-1 ANN models developed in the present study can accurately predict the component dynamic amplification factors (CDAF) using various input parameters.

The observations made during this research are confined to the examined buildings and the ground motions. A comprehensive research study is encouraged by considering the various low- and high-rise buildings in generalizing the findings. This study is limited to only the five-story building structure and mass irregularity as a preliminary investigation. The nonlinear behavior of the building model needs to be considered for more generalized results. A future investigation can be extended to study high-rise structures with different irregularities (e.g., stiffness and vertical geometric).

Author Contributions: Conceptualization, S.P.C. and D.-P.N.K.; methodology, S.P.C. and D.-P.N.K.; software, S.P.C., D.-P.N.K., A.K.S. and M.J.; formal analysis, S.P.C. and D.-P.N.K.; writing—original draft preparation, S.P.C., D.-P.N.K., I.H., U.R. and M.J.; writing—review and editing, S.P.C. and D.-P.N.K.; supervision, S.P.C. and D.-P.N.K.; project administration, D.-P.N.K. All authors have read and agreed to the published version of the manuscript.

Institutional Review Board Statement: Not applicable.

Informed Consent Statement: Not applicable.

Data Availability Statement: Data are available within the article.

Conflicts of Interest: The authors declare no conflict of interest.

References

1. Filiatrault, A.; Sullivan, T. Performance-based seismic design of nonstructural building components: The next frontier of earthquake engineering. *Earthq. Eng. Eng. Vib.* **2014**, *13*, 17–46. [CrossRef]
2. Shang, Q.; Wang, T.; Li, J. Seismic fragility of flexible pipeline connections in a base isolated medical building. *Earthq. Eng. Eng. Vib.* **2019**, *18*, 903–916. [CrossRef]
3. Di Sarno, L.; Magliulo, G.; D'Angela, D.; Cosenza, E. Experimental assessment of the seismic performance of hospital cabinets using shake table testing. *Earthq. Eng. Struct. Dyn.* **2019**, *48*, 103–123. [CrossRef]
4. Anajafi, H.; Medina, R. Evaluation of ASCE 7 equations for designing acceleration-sensitive nonstructural components using data from instrumented buildings. *Earthq. Eng. Struct. Dyn.* **2018**, *47*, 1075–1094. [CrossRef]
5. Suarez, L.E.; Singh, M.P. Floor response spectra with structure–equipment interaction effects by a mode synthesis approach. *Earthq. Eng. Struct. Dyn.* **1987**, *15*, 141–158. [CrossRef]
6. Adam, C. Dynamics of Elastic–Plastic Shear Frames with Secondary Structures: Shake Table and Numerical Studies. *Earthq. Eng. Struct. Dyn.* **2001**, *30*, 257–277. [CrossRef]

7. Menon, A.; Magenes, G. Definition of Seismic Input for Out-of-Plane Response of Masonry Walls: II. Formulation. *J. Earthq. Eng.* **2011**, *15*, 195–213. [CrossRef]

8. Challagulla, S.P.; Bhargav, N.C.; Parimi, C. Evaluation of Damping Modification Factors for Floor Response Spectra via Machine Learning Model. In *Structures*; Elsevier: Amsterdam, The Netherlands, 2022; Volume 39, pp. 679–690.

9. D'Angela, D.; Magliulo, G.; Cosenza, E. Seismic damage assessment of unanchored nonstructural components taking into account the building response. *Struct. Saf.* **2021**, *93*, 102126. [CrossRef]

10. Vukobratović, V.; Fajfar, P. A method for the direct determination of approximate floor response spectra for SDOF inelastic structures. *Bull. Earthq. Eng.* **2015**, *13*, 1405–1424. [CrossRef]

11. Jiang, W.; Li, B.; Xie, W.-C.; Pandey, M.D. Generate floor response spectra: Part 1. Direct spectra-to-spectra method. *Nucl. Eng. Des.* **2015**, *293*, 525–546. [CrossRef]

12. Calvi, P.M.; Sullivan, T.J. Estimating floor spectra in multiple degree of freedom systems. *Earthq. Struct.* **2014**, *7*, 17–38. [CrossRef]

13. Zhai, C.-H.; Zheng, Z.; Li, S.; Pan, X.; Xie, L.-L. Seismic response of nonstructural components considering the near-fault pulse-like ground motions. *Earthq. Struct.* **2016**, *10*, 1213–1232. [CrossRef]

14. Petrone, C.; Magliulo, G.; Manfredi, G. Floor response spectra in RC frame structures designed according to Eurocode 8. *Bull. Earthq. Eng.* **2016**, *14*, 747–767. [CrossRef]

15. Berto, L.; Bovo, M.; Rocca, I.; Saetta, A.; Savoia, M. Seismic safety of valuable non-structural elements in RC buildings: Floor Response Spectrum approaches. *Eng. Struct.* **2020**, *205*, 110081. [CrossRef]

16. Landge, M.V.; Ingle, R.K. Comparative study of floor response spectra for regular and irregular buildings subjected to earthquake. *Asian J. Civ. Eng.* **2021**, *22*, 49–58. [CrossRef]

17. Singh, M.P.; Suarez, L.E. Seismic response analysis of structure–equipment systems with non-classical damping effects. *Earthq. Eng. Struct. Dyn.* **1987**, *15*, 871–888. [CrossRef]

18. Shang, Q.; Li, J.; Wang, T. Floor acceleration response spectra of elastic reinforced concrete frames. *J. Build. Eng.* **2022**, *45*, 103558. [CrossRef]

19. Li, B.; Jiang, W.; Xie, W.-C.; Pandey, M.D. Generate floor response spectra, Part 2: Response spectra for equipment-structure resonance. *Nucl. Eng. Des.* **2015**, *293*, 547–560. [CrossRef]

20. Dexter, A. Advances in characterization of soil structure. *Soil Tillage Res.* **1988**, *11*, 199–238. [CrossRef]

21. Mercado, F.J.V.; Azizsoltani, H.; Gaxiola-Camacho, J.R.; Haldar, A. Seismic Reliability Evaluation of Structural Systems for Different Soil Conditions. *Int. J. Geotech. Earthq. Eng.* **2017**, *8*, 23–38. [CrossRef]

22. Kumar, M.; Mishra, S.S. Study of seismic response characteristics of building frame models using shake table test and considering soil–structure interaction. *Asian J. Civ. Eng.* **2019**, *20*, 409–419. [CrossRef]

23. Boulkhiout, R.; Messast, S. Effect of Soil on the Seismic Response of Structures Taking Into Consideration Soil-Structure Interaction. *Int. J. Geotech. Earthq. Eng.* **2020**, *11*, 72–90. [CrossRef]

24. Hassan, A.; Pal, S. Effect of soil condition on seismic response of isolated base buildings. *Int. J. Adv. Struct. Eng.* **2018**, *10*, 249–261. [CrossRef]

25. Jayalekshmi, B.R.; Chinmayi, H.K. Effect of soil stiffness on seismic response of reinforced concrete buildings with shear walls. *Innov. Infrastruct. Solutions* **2016**, *1*, 2. [CrossRef]

26. Ceroni, F.; Sica, S.; Pecce, M.; Garofano, A. Effect of Soil-Structure Interaction on the Dynamic Behavior of Masonry and RC Buildings. In Proceedings of the 15th World Conference on Earthquake Engineering (WCEE), Lisbon, Portugal, 24–28 September 2012.

27. Choi, Y.; Ju, H.; Jung, H.-J. Floor Response Spectrum of Nuclear Power Plant Structure Considering Soil-Structure Interaction. In *Vibration Engineering for a Sustainable Future*; Springer: Berlin/Heidelberg, Germany, 2021; pp. 161–166.

28. Surana, M.; Singh, Y.; Lang, D.H. Effect of structural characteristics on damping modification factors for floor response spectra in RC buildings. *Eng. Struct.* **2021**, *242*, 112514. [CrossRef]

29. Adam, C.; Furtmüller, T.; Moschen, L. Floor Response Spectra for Moderately Heavy Nonstructural Elements Attached to Ductile Frame Structures. In *Computational Methods in Earthquake Engineering*; Springer: Berlin/Heidelberg, Germany, 2013; pp. 69–89.

30. *Indian Standard (IS), IS 1893 (Part 1)*; Criteria for Earthquake Resistant Design of Structures, Part-1, General Provisions and Building. Sixth Revision. Bureau of Indian Standards: New Delhi, India, 2016.

31. *Indian Standard (IS), IS 875 (Part 2)–1987 (Reaffirmed 1997)*; Code of Practice for Design Loads (Other Than Earthquake) for Buildings and Structures, Part 2. Bureau of Indian Standards: New Delhi, India, 1998.

32. *SAP2000®Version 17*; Integrated Software for Structural Analysis and Design, Computers and Structures, Inc.: Walnut Creek, CA, USA; New York, NY, USA, 2015.

33. Surana, M.; Singh, Y.; Lang, D.H. Effect of irregular structural configuration on floor acceleration demand in hill-side buildings. *Earthq. Eng. Struct. Dyn.* **2018**, *47*, 2032–2054. [CrossRef]

34. Biggs, J.M.; Rosset, J.M. *Seismic Analysis of Equipment Mounted on a Massive Structure, Seismic Design for Nuclear Power Plants*; Hansen, R.J., Ed.; Mass: Cambridge, UK, 1970.

35. Bagheri, B.; Nivedita, K.A.; Firoozabad, E.S. Comparative Damage Assessment of Irregular Building Based on Static and Dynamic Analysis. *Int. J. Civ. Struct. Eng.* **2013**, *3*, 505.

36. Senaldi, I.E.; Magenes, G.; Penna, A.; Galasco, A.; Rota, M. The Effect of Stiffened Floor and Roof Diaphragms on the Experimental Seismic Response of a Full-Scale Unreinforced Stone Masonry Building. *J. Earthq. Eng.* **2014**, *18*, 407–443. [CrossRef]

37. PEER Ground Motion Database. Pacific Earthquake Engineering Research Center. University of California, Berkeley, CA, USA, 2013. Available online: http://ngawest2.berkeley.edu (accessed on 1 October 2022).
38. American Society of Civil Engineers (ASCE). *Minimum Design Loads and Associated Criteria for Buildings and Other Structures, ASCE 7-16*; American Society of Civil Engineers: Reston, VA, USA, 2017.
39. *NEHRP Recommended Seismic Provisions for New Buildings and Other Structures (FEMA P-750)*; Federal Emergency Management Agency, Building Seismic Safety Council: Washington, DC, USA, 2009.
40. Khy, K.; Chintanapakdee, C.; Wijeyewickrema, A.C. Application of Conditional Mean Spectrum in Nonlinear Response History Analysis of Tall Buildings on Soft Soil. *Eng. J.* **2019**, *23*, 135–150. [CrossRef]
41. Al Atik, L.; Abrahamson, N. An Improved Method for Nonstationary Spectral Matching. *Earthq. Spectra* **2010**, *26*, 601–617. [CrossRef]
42. Seismosoft. SeismoMatch—A Computer Program for Spectrum Matching of Earthquake Records, 2020. Available online: https://seismosoft.com/products/seismomatch/ (accessed on 1 October 2022).
43. *Eurocode 8: Design of Structures for Earthquake Resistance-Part 1: General Rules, Seismic Actions and Rules for Buildings*; European Committee for Standardization: Brussels, Belgium, 2005.
44. *Chinese Standard 50011-2010*; Code for Seismic Design of Buildings. Ministry of Housing and Urban-Rural Development: Beijing, China, 2010.
45. Aragaw, L.F.; Calvi, P.M. Earthquake-Induced Floor Accelerations in Base-Rocking Wall Buildings. *J. Earthq. Eng.* **2021**, *25*, 941–969. [CrossRef]
46. Flood, I.; Christophilos, P. Modeling construction processes using artificial neural networks. *Autom. Constr.* **1996**, *4*, 307–320. [CrossRef]
47. Flood, I.; Kartam, N. Neural Networks in Civil Engineering. II: Systems and Application. *J. Comput. Civ. Eng.* **1994**, *8*, 149–162. [CrossRef]
48. Jeng, D.S.; Cha, D.H.; Blumenstein, M. Application of Neural Network in Civil Engineering Problems. In Proceedings of the International Conference on Advances in the Internet, Processing, Systems and Interdisciplinary Research, Sveti Stefan, Montenegro, 5–11 October 2003.
49. Shahin, M.A.; Jaksa, M.B.; Maier, H.R. Artificial Neural Network-Based Settlement Prediction Formula for Shallow Foundations on Granular Soils. *Aust. Geomech. J.* **2002**, *37*, 45–52.
50. Challagulla, S.P.; Parimi, C.; Pradeep, S.; Farsangi, E. Estimation of dynamic design parameters for buildings with multiple sliding non-structural elements using machine learning. *Int. J. Struct. Eng.* **2021**, *11*, 147–172. [CrossRef]
51. Challagulla, S.P.; Parimi, C.; Anmala, J. Prediction of Spectral Acceleration of a Light Structure with a Flexible Secondary System Using Artificial Neural Networks. *Int. J. Struct. Eng.* **2020**, *10*, 353–379. [CrossRef]
52. Hornik, K.; Stinchcombe, M.; White, H. Multilayer feedforward networks are universal approximators. *Neural Netw.* **1989**, *2*, 359–366. [CrossRef]
53. Acharyya, R.; Dey, A. Assessment of bearing capacity for strip footing located near sloping surface considering ANN model. *Neural Comput. Appl.* **2019**, *31*, 8087–8100. [CrossRef]
54. Bhargav, N.C.; Challagulla, S.P.; Farsangi, E.N. Prediction Model for Significant Duration of Strong Motion in India. *J. Appl. Sci. Eng.* **2022**, *26*, 279–292.